THE JOURNAL OF BIOLOGICAL CHEMISTRY VOL. 288, NO. 13, pp. 9238–9248, March 29, 2013

Dimerization of Bacterial Diaminopimelate Epimerase Is Essential for Catalysis*

Received for publication, January 2, 2013, and in revised form, February 7, 2013 Published, JBC Papers in Press, February 19, 2013, DOI 10.1074/jbc.M113.450148

Lilian Hor[‡§¶‖], Renwick C. J. Dobson[§‖1], Matthew T. Downton[‡‡], John Wagner[‡‡], Craig A. Hutton[¶‖], and Matthew A. Perugini[‡§‖2]**

*From the [‡]Department of Biochemistry, La Trobe Institute for Molecular Science, La Trobe University, Melbourne, Victoria 3086, Australia, [§]Department of Biochemistry and Molecular Biology and [¶]School of Chemistry, The University of Melbourne, Parkville, Victoria 3010, Australia, [‖]Bio21 Molecular Science and Biotechnology Institute, Parkville, Victoria 3010, Australia, **Biomolecular Interaction Centre and School of Biological Sciences, The University of Canterbury, Private Bag 4800, Christchurch, New Zealand, and [‡‡]IBM Research Collaboratory for Life Sciences-Melbourne, Victorian Life Sciences Computation Initiative, The University of Melbourne, Victoria 3010, Australia*

Background: Diaminopimelate epimerase catalyzes a key step in the synthesis of *meso*-diaminopimelate and lysine.
Results: Solution and crystal studies show that diaminopimelate epimerase exists as an active dimer, whereas a monomeric mutant is catalytically inactive.
Conclusion: The diaminopimelate epimerase dimer is essential for function with evidence suggesting that dimerization attenuates subunit dynamics.
Significance: Structural insights into the design of antimicrobial agents to disrupt diaminopimelate epimerase dimerization are provided.

Diaminopimelate (DAP) epimerase is involved in the biosynthesis of *meso*-DAP and lysine, which are important precursors for the synthesis of peptidoglycan, housekeeping proteins, and virulence factors in bacteria. Accordingly, DAP epimerase is a promising antimicrobial target. Previous studies report that DAP epimerase exists as a monomeric enzyme. However, we show using analytical ultracentrifugation, X-ray crystallography, and enzyme kinetic analyses that DAP epimerase from *Escherichia coli* exists as a functional dimer in solution and the crystal state. Furthermore, the 2.0-Å X-ray crystal structure of the *E. coli* DAP epimerase dimer shows for the first time that the enzyme exists in an open, active conformation. The importance of dimerization was subsequently probed by using site-directed mutagenesis to generate a monomeric mutant (Y268A). Our studies show that Y268A is catalytically inactive, thus demonstrating that dimerization of DAP epimerase is essential for catalysis. Molecular dynamics simulations indicate that the DAP epimerase monomer is inherently more flexible than the dimer, suggesting that dimerization optimizes protein dynamics to support function. Our findings offer insight into the development of novel antimicrobial agents targeting the dimeric antibiotic target DAP epimerase.

Diaminopimelate (DAP)[3] epimerase (EC 5.1.1.7) is a member of the pyridoxal 5′-phosphate-independent amino acid racemases. It catalyzes the stereoinversion of LL-DAP to *meso*-DAP in the lysine biosynthetic pathway in plants and bacteria (1–3). The products of this pathway, namely *meso*-DAP and lysine, are used in the cross-linking of the peptidoglycan cell wall of Gram-negative and Gram-positive bacteria, respectively. Lysine is also an important building block for the synthesis of housekeeping proteins and virulence factors (1–3). Consequently, DAP epimerase represents a promising target for the development of novel antimicrobial agents (4, 5).

DAP epimerase catalyzes the conversion of LL-DAP to *meso*-DAP using a two-base mechanism involving a pair of cysteine residues (Fig. 1) (6–8). The first cysteine is present in the thiolate form and acts as a base and abstracts a proton from LL-DAP, whereas the second cysteine acts as an acid and reprotonates the molecule, giving *meso*-DAP. The reaction goes through a planar carbanion-like transition state (Fig. 1).

Previous studies of DAP epimerase have reported a monomeric enzyme that adopts a symmetrical α/β domain structure with each domain contributing one of the two key active site cysteine residues located in the interdomain cleft (8–12). This unique fold was first observed for the *Haemophilus influenzae* enzyme and is now referred to as the DAP epimerase-like fold (9). Since the first structure of DAP epimerase was solved in 1998 (9), a number of structures have been determined that adopt the DAP epimerase-like fold. These include proline racemase (13), the isomerases PrpF (14, 15) and 3-methylitaconate Δ-isomerase (16), PhzF (17), and proteins of unknown or unconfirmed function (18, 19). Interestingly, the majority of these proteins have been found to adopt a dimeric quaternary

* This work was supported in part by Victorian Life Sciences Computation Initiative Grant VR0089 to its Peak Computing Facility at the University of Melbourne, an initiative of the Victorian Government, Australia.
The atomic coordinates and structure factors (codes 4IJZ and 4IK0) have been deposited in the Protein Data Bank (http://wwpdb.org/).
[1] Supported by the University of Melbourne C. R. Roper Fellowship.
[2] Supported by Australian Research Council for Future Fellowship FT0991245.
To whom correspondence should be addressed: Dept. of Biochemistry, La Trobe Inst. for Molecular Science, La Trobe University, Melbourne, Victoria 3086, Australia. Tel.: 61-3-9479-6570; Fax: 61-3-9479-1266; E-mail: M. Perugini@latrobe.edu.au.

[3] The abbreviations used are: DAP, diaminopimelate; PISA, Protein Interfaces, Surfaces and Assemblies; Bis-tris propane, 1,3-bis[tris(hydroxymethyl)-methylamino]propane.

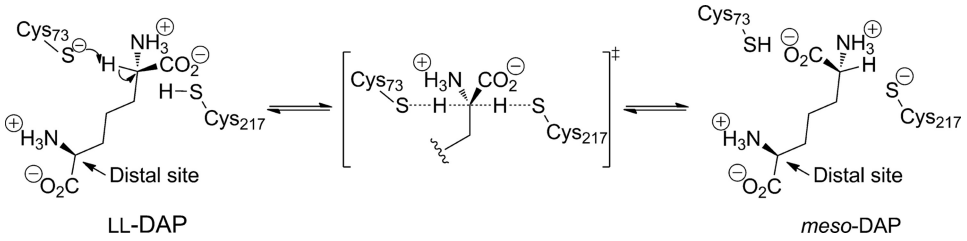

FIGURE 1. **Reaction catalyzed by DAP epimerase and its mechanism.**

structure with dimerization occurring through the N-terminal domain (13–15, 17–19).

Although previous studies of DAP epimerase suggest that the enzyme is monomeric (9, 11, 12), computational analyses of the crystal structures using Protein Interfaces, Surfaces and Assemblies (PISA) (20) suggest that the enzyme could adopt a dimeric architecture similar to the dimer observed in other DAP epimerase-like fold proteins. We therefore set out to examine the quaternary structure of bacterial DAP epimerase both in solution and the crystal state using the enzyme from *Escherichia coli*. In addition, we compared the function of the wild-type dimer and a monomeric mutant of *E. coli* DAP epimerase generated via site-directed mutagenesis.

Our studies reveal that DAP epimerase is a dimer in solution and the crystal state. The high resolution crystal structure of *E. coli* DAP epimerase shows that the dimeric enzyme adopts an open, active conformation not previously reported in the literature. Furthermore, mutagenesis studies targeting Tyr^{268} at the dimer interface yield a monomeric mutant (Y268A) that is catalytically inactive, demonstrating for the first time that dimerization of DAP epimerase is critical for catalysis.

EXPERIMENTAL PROCEDURES

Protein Expression and Purification—E. coli DAP epimerase was expressed and purified as described in Hor *et al.* (21), and the *H. influenzae* ortholog was expressed and purified as described in Cirilli *et al.* (9) with the exclusion of the ammonium sulfate precipitation step.

Generation of E. coli DAP Epimerase Mutant—The point mutation in the *E. coli dapF* gene contained in pET11a (21) was introduced using the QuikChange II XL site-directed mutagenesis kit (Stratagene). The primer set 5′-GGCGGTACATGTCTACGCCGGATTTATTCATCTAC-3′ and 5′-GTAGATGAATAAATCCGGCGTAGACATGTACCGCC-3′ was designed to introduce the Y268A amino acid substitution. Mutagenesis was performed according to the manufacturer's instructions with successful mutation confirmed by dideoxynucleotide sequencing. The mutant was expressed at 16 °C in autoinduction medium (22) and purified using the same protocol as for the wild-type enzyme (21).

Mass Spectrometry—Mass spectrometric analyses were performed on an Agilent 6220 Accurate-Mass TOF LC/MS mass spectrometer coupled to an Agilent 1100 LC system (Agilent, Palo Alto, CA) as described previously (23, 24). Protein samples were left in their original buffer (typically 20 mM Tris, 150 mM NaCl, pH 8.0) and were loaded onto an Agilent Poroshell 300SB-C18 2.1 × 75-mm, 5-μm reverse phase column attached to the mass spectrometer.

Circular Dichroism Spectroscopy—CD spectroscopy was performed using an AVIV 410-SF CD spectrometer as reported previously (25–27). Wavelength spectra were collected between 190 and 250 nm in 20 mM Tris, 150 mM NaCl, 1 mM tris(2-carboxyethyl)phosphine, pH 7.8 with 0.15 mg ml^{-1} enzyme using 1-mm quartz cuvettes with a step size of 0.5 nm and 2-s averaging time. Data were analyzed using the CONTINLL algorithm from the CDPro software package (28) using the SP43 database.

Analytical Ultracentrifugation—Absorbance-based sedimentation velocity and sedimentation equilibrium experiments were performed in a Beckman XL-I analytical ultracentrifuge with a four-hole An-60 Ti or eight-hole An-50 Ti rotor at 20 °C as described previously (26, 27, 29, 30). For sedimentation velocity experiments, double sector quartz cells were loaded with 380 μl of sample and 400 μl of reference (20 mM Tris, 150 mM NaCl, 1 mM tris(2-carboxyethyl)phosphine, pH 7.8) with data collected at 40,000 or 50,000 rpm. For sedimentation equilibrium experiments, quartz cells were loaded with 100 μl of sample and 120 μl of reference (20 mM Tris, 150 mM NaCl, 1 mM tris(2-carboxyethyl)phosphine, pH 7.8) with data collected at 10,000 and 16,000 rpm. Sedimentation velocity data were fitted with a continuous size distribution model using SEDFIT (31) or the enhanced van Holde-Weischet method (32) using UltraScan III (33, 34). Sedimentation equilibrium data were fitted to a monomer-dimer self-association model using SEDPHAT (35). Bead modeling was conducted using the SOMO method incorporated in the UltraScan III software suite (36, 37).

Enzyme Kinetic Assays—Enzyme activity of DAP epimerase was determined using the modified DAP epimerase-DAP dehydrogenase coupled spectrophotometric assay (38). Briefly, to an assay containing buffer, DAP and $NADP^+$ were added to DAP dehydrogenase whereby an increase at 340 nm was observed until a plateau was attained that corresponded to the conversion of *meso*-DAP to tetrahydrodipicolinate until *meso*-DAP was depleted. DAP epimerase was then added to the resulting mixture, and the resulting rate was recorded. Assays were performed at 30 °C in a temperature-controlled Varian Cary 4000 UV spectrophotometer and incubated for 12 min before initiation of the reaction with enzyme. Assays were performed in duplicate or triplicate. A typical assay contained 100 mM Tris, pH 7.8, 0.1 mM LL-DAP, 0.44 mM $NADP^+$, 1 mM DTT, 1.8 μM DAP dehydrogenase, and DAP epimerase.

X-ray Crystallography—The crystallization, data collection, and structure determination of wild-type *E. coli* DAP epimerase have been described previously (21). Y268A was

TABLE 1

Refinement statistics for *E. coli* DAP epimerase wild-type structure (Protein Data Bank code 4IJZ) and Y268A mutant (Protein Data Bank code 4IK0)

r.m.s.d., root mean square deviation.

	Wild-type	Y268A
Data collection		
Space group	$P4_12_12$	$P4_12_12$
Cell parameters		
a, b, c (Å)	89.4, 89.4, 179.6	89.2, 89.2, 179.5
α, β, γ (°)	90.0, 90.0, 90.0	90.0, 90.0, 90.0
Resolution (Å)	44.69–2.00 (2.11–2.00)	51.59–2.05 (2.16–2.05)
Observed reflections	215,760 (29,012)	290,926 (42,700)
Unique reflections	47,663 (6,683)	46,324 (6,635)
Completeness (%)	96.1 (93.7)	100.0 (100.0)
R_{merge} [a]	0.077 (0.339)	0.126 (0.577)
R_{pim} [b]	0.039 (0.137)	0.055 (0.246)
R_{rim}	0.087 (0.385)	0.137 (0.628)
Mean $I/\sigma(I)$	13.0 (4.2)	10.4 (3.2)
Redundancy	4.5 (4.3)	6.3 (6.4)
Wilson B value (Å^2)	23.4	25.0
Molecules in asymmetric unit	2	2
V^M (Å^3 Da^{-1})	2.89	2.89
Solvent content (%)	57	57
Refinement		
Resolution	44.37–2.00 (2.05–2.00)	49.68–2.05 (2.10–2.05)
R_{work} [c]	0.161 (0.215)	0.176 (0.210)
R_{free} [c,d]	0.200 (0.260)	0.217 (0.239)
No. atoms		
Protein	4,289	4,240
Ligands	12	13
Water	516	395
Mean B value (Å^2)		
Main chain	22.4	23.6
Side chain	25.9	26.1
Ligands	46.0	52.7
Water	37.3	35.5
r.m.s.d. from ideality		
Bond length (Å)	0.014	0.014
Bond angles (°)	1.64	1.65
Ramachandran statistics (%)		
Most favored regions	97.3	98.2
Additionally allowed regions	2.7	1.6
Disallowed regions	0.0	0.2

[a] $R_{merge} = \sum_h \sum_i |I_i(h) - I(h)| / \sum_h \sum_i I_i(h)$.
[b] $R_{pim} = \sum_h [1/(N-1)]^{1/2} \sum_i |I_i(h) - I(h)| / \sum_h \sum_i I_i(h)$.
[c] $R = \Sigma ||F_{obs}| - |F_{calc}|| / \Sigma |F_{obs}|$ where F_{obs} and F_{calc} are the observed and calculated structure factor amplitudes, respectively.
[d] R_{free} was calculated with 5% of the diffraction data and was selected randomly and omitted from the refinement. For the Y268A structure, the same 5% set of diffraction data was used as the wild-type *E. coli* DAP epimerase structure.

crystallized using the hanging drop vapor diffusion method with drops containing 2 μl of protein solution (8.0 mg ml^{-1} in 20 mM Tris, 5 mM DTT, 5 mM tris(2-carboxyethyl)phosphine, pH 7.8) and 2 μl of precipitant solution (0.2 M sodium iodide, 18% (w/v) PEG 3350, 0.1 M Bis-tris propane, pH 6.5, 5 mM DAP) at 20 °C.

For x-ray data collection, the Y268A crystal was soaked in cryoprotectant solution containing reservoir solution made up in glycerol (20%, v/v) and directly flash cooled in liquid nitrogen. Intensity data were collected at −163 °C at the Australian Synchrotron (MX2 beamline). Data were collected in 0.5° oscillations for 250° using an ADSC Q315r image plate detector positioned 300 mm from the crystal with an exposure time of 0.5 s and 80% attenuation. The diffraction data were processed using the programs MOSFLM (39) and SCALA (40). Although 250° of data were initially collected, the resolution and the quality of the diffraction data decreased (as judged by an increased batch R_{merge}); as such, only the first 80° data were analyzed. The Y268A structure was solved by molecular replacement using Phaser (41) using the wild-type *E. coli* DAP epimerase (Protein Data Bank code 4IJZ) as the search model.

Structural refinement of both wild-type and mutant structures was performed using REFMAC5 (40) and iterative model building with WINCOOT (42). Translation Libration Screw-motion refinement in REFMAC (43) was applied in the final rounds of refinement using three groups as determined using TLSMD (44, 45). Structure quality was assessed by the program MolProbity (46). X-ray data collection and refinement statistics for wild-type *E. coli* DAP epimerase and Y268A mutant structures are shown in Table 1. Interface analysis used PISA at the European Bioinformatics Institute authored by Krissinel and Henrick (20).

Molecular Dynamic Simulations—Simulations of the wild-type *E. coli* DAP epimerase crystal structure dimer and the monomer corresponding to chain A of the dimer were performed in the NPT ensemble at a temperature of 298 K and pressure of 1 atm using the molecular dynamics program NAMD (47). The CHARMM force field was used with CMAP corrections to backbone dihedral interactions (48). Cys-73 was deprotonated using the patch of Foloppe *et al.* (49). All simulations were solvated with TIP3P water, and ions were added at a concentration of 150 mM NaCl. A simulation time step of 2 fs was used with a total simulation length of 25 ns.

TABLE 2

Secondary structure analysis of *E. coli* wild-type and mutant DAP epimerase

CD data were analyzed using CDPro (28) with the CONTINLL algorithm and the SP43 reference database. r.m.s.d., root mean square deviation.

	α-Helix	β-Strand	Turn	Random	r.m.s.d.
	%	%	%	%	
WT	18	31	21	30	0.059
Y268A	17	31	23	29	0.069

RESULTS

DAP Epimerase Is Dimeric in Solution—E. coli DAP epimerase was expressed and purified as described elsewhere (21). The enzyme was initially characterized by electrospray ionization-TOF MS to show that the mass of the recombinant protein (31.031.1 Da) was consistent with that of the amino acid sequence. CD spectroscopy showed that the enzyme was folded (Table 2), and subsequent analysis using the DAP epimerase-DAP dehydrogenase coupled assay (38) indicated that the enzyme was active (data not shown).

The quaternary structure of *E. coli* DAP epimerase was assessed by sedimentation velocity experiments performed in the analytical ultracentrifuge. The raw data (Fig. 2*A*) were fitted to an enhanced van Holde-Weischet model (32), indicating that *E. coli* DAP epimerase sediments with a standardized sedimentation coefficient ($s_{20,w}$) of 4.3 S (Fig. 2*B*). This was complementary to the result obtained using the $c(s)$ distribution (31, 50) (see Fig. 6*A*). Conversion of the $c(s)$ profile to a $c(M)$ distribution yields an apparent molecular mass of 61.3 kDa, which is consistent with *E. coli* DAP epimerase being a dimer in solution (Table 3).

To determine the dimerization affinity of wild-type *E. coli* DAP epimerase, sedimentation equilibrium experiments were performed in the analytical ultracentrifuge at two rotor speeds (10,000 and 16,000 rpm) and various protein concentrations (0.32, 0.64, 1.9, and 5.8 μM). The resulting data were fitted by global nonlinear regression analyses to a monomer-dimer equilibrium, which yielded a dimer-monomer dissociation constant ($K_D^{2\rightarrow1}$) of 22 nM (Table 3 and Fig. 3).

In addition, sedimentation velocity experiments on the most well characterized DAP epimerase from *H. influenzae* (8–10, 51, 52) showed that this enzyme is also dimeric in solution with a standardized sedimentation coefficient ($s_{20,w}$) of 4.1 S (Table 3 and Fig. 2, *C* and *D*). This result is consistent with the quaternary structure of *E. coli* DAP epimerase (and other proteins that adopt the DAP epimerase-like fold) and suggests that a dimer may be the true biologically relevant form.

E. coli DAP Epimerase Crystal Structure—We next set out to generate high resolution structural information for the *E. coli* DAP epimerase dimer. The recombinant enzyme was crystallized as reported recently (21), and the x-ray crystal structure was determined in the space group $P4_12_12$ to a resolution of 2.0 Å by molecular replacement (Protein Data Bank code 4IJZ) (Fig. 4). The Ramachandran plot has 97.3% of residues in the most favored regions, 2.7% in the additionally allowed regions, and no residues in the disallowed regions. As expected, the structure adopts the DAP epimerase-like fold similarly to several other homologs (9–12).[4] The monomer comprises two symmetrical domains with each domain consisting of a central α-helix surrounded by eight β-strands (Fig. 4*B*). These domains show pseudosymmetry with the N-terminal domain (residues 1–119 and 263–274) and C-terminal domain (residues 120–262) and are structurally similar with an root mean square deviation of 2.67 Å over 93 α-carbon pairs with ~18% sequence identity between the two domains. Consistent with solution study results, *E. coli* DAP epimerase crystallized as a dimer in the asymmetric unit with the dimeric architecture structurally akin to DAP epimerase-like proteins with oligomerization taking place at the N-terminal domain (Fig. 4*A*).

Significantly, the structure of *E. coli* DAP epimerase also crystallized in the open conformation with the two active site Cys residues existing in the non-disulfide-bonded reduced form with 9.5 and 13.3 Å between Cys residues in monomers A and B, respectively (Fig. 4, *B* and *C*). Accordingly, this crystal structure represents an active conformation of the enzyme (Fig. 4, *B* and *C*). This is in contrast to the inactive conformation observed in *H. influenzae* (Protein Data Bank codes 1BWZ and 1GQZ) and *Mycobacterium tuberculosis* DAP epimerase (Protein Data Bank code 3FVE) where a disulfide bridge between the active site Cys residues is observed (9–11). Only one other DAP epimerase structure, from *Bacillus anthracis* (Protein Data Bank code 2OTN), has been crystallized in the open conformation.[4]

Interestingly, SOMO bead model analysis (36, 37) of the dimer results in a computed sedimentation coefficient of 4.3 S and a frictional ratio of 1.3, which are identical to the experimentally determined values (Table 3). This suggests that the open dimer conformation observed in the crystal structure also forms in aqueous solution.

Active Site—The active site of *E. coli* DAP epimerase resides in a cleft between the two domains with each domain contributing one of the cysteine residues important for catalysis (Fig. 4, *B* and *C*). Superimposition of the active sites of *E. coli* and *B. anthracis* DAP epimerase structures indicates that the majority of active site residues are similarly oriented (Fig. 4*C*). However, minor changes are observed for Cys^{73}, Gly^{74}, and Asn^{75}. The different arrangement of these residues can be explained by their location in the sequence. Cys^{73}–Asn^{75} are located on a dynamic loop (51), which means there is increased flexibility in this region. This is supported by the higher temperature factor of these three residues of 35.2 $Å^2$ compared with the average *B* factor for all residues of 21.8 $Å^2$.

Dimer Interface—As for other proteins that adopt the DAP epimerase-like fold, the dimerization interface of *E. coli* DAP epimerase occurs between the N-terminal domains of the two monomers. The dimer interface of *E. coli* DAP epimerase buries 765 $Å^2$ per monomer, which represents 6.1% of the total surface area of each monomer. This is similar to the *H. influenzae* and *B. anthracis* orthologs but is markedly less than other DAP epimerase-like fold proteins (Table 4). Analysis by PISA (20) reveals that the *E. coli* DAP epimerase dimer interface is

[4] M. H. Matho, K. Fukuda, E. Santelli, K. Jaroszewski, R. C. Liddington, and D. I. Roper, unpublished data.

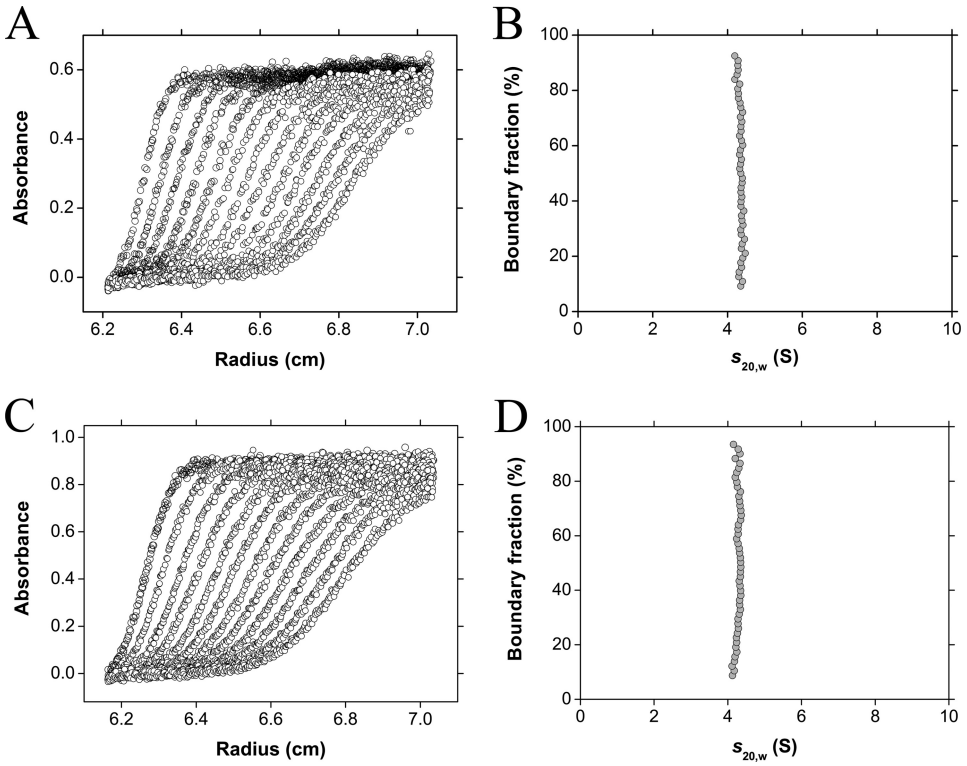

FIGURE 2. **Sedimentation velocity analysis of *E. coli* and *H. influenzae* DAP epimerase.** *A*, *E. coli* DAP epimerase sedimentation velocity raw data. Absorbance at 227 nm plotted as a function of radial position from the axis of rotation (cm) is shown. The raw data are presented as *open circles*. *B*, enhanced van Holde-Weischet integral distribution plot from extrapolation of *E. coli* DAP epimerase sedimentation velocity raw data shown in *A*. *C*, *H. influenzae* DAP epimerase sedimentation velocity raw data. Absorbance at 226 nm plotted as a function of radial position from the axis of rotation (cm) is shown. The raw data are presented as *open circles*. *D*, enhanced van Holde-Weischet integral distribution plot from extrapolation of *H. influenzae* DAP epimerase sedimentation velocity raw data shown in *C*.

TABLE 3

Summary of hydrodynamic properties of *E. coli* DAP epimerase and Y268A mutant

DAP epimerase	Theoretical molecular mass[a]	$s_{20,w}$	f/f_0[b]	Experimental molecular mass[c]	$K_D^{2\rightarrow1}$
	kDa	*S*		*kDa*	
E. coli	62.0	4.3	1.3	61.3	22 nM
H. influenzae	60.5	4.1	1.3	59.3	ND[d]
Y268A	61.9	2.9	1.2	29.9	54 μM

[a] Molecular mass of a dimer based on amino acid composition.
[b] Frictional ratio derived using the ν bar method.
[c] Molecular mass derived experimentally using $c(M)$ analysis.
[d] Not determined.

composed of 13 hydrogen bonds and seven salt bridges. The locations of these interactions are depicted in Fig. 4, *D* and *E*.

The *E. coli* DAP epimerase dimer interface is contributed by three areas of the protein: residues 3–12 (N terminus), residues 36–43 (loop), and residues 266–273 (C terminus) (Fig. 4*E*). Residues of the C terminus, which form part of the N-terminal domain and represent the final β-strand of the monomer, interact in an antiparallel manner, creating a continuous β-sheet that weaves through the entire *E. coli* DAP epimerase dimer (Fig. 4*A*).

Engineering a Monomeric Variant—To probe the importance of dimerization, a point mutation targeting Tyr^{268} at the dimer interface was created. Care was taken in selecting Tyr^{268} because this residue is not close to the active site and would be unlikely to perturb the catalytic function of the enzyme. Interestingly, Tyr^{268} is involved in hydrogen bonding at the dimer interface with the same residue from the neighboring monomer. Therefore, Tyr^{268} was mutated to Ala, yielding the point mutant referred to herein as Y268A.

Y268A was found to be of the expected molecular mass (30,940.0 Da) as determined by mass spectrometry and shown by CD spectroscopy to have secondary structure proportions similar to those of the wild-type enzyme (Table 2). In addition, the crystal structure of Y268A (Protein Data Bank code 4IK0) was determined to 2.05-Å resolution, clearly showing that the Tyr to Ala mutation at position 268 was successful (Fig. 5*A*). In addition, x-ray crystallographic studies show that Y268A retains the secondary and tertiary structure of the wild-type enzyme with superimposition of the mutant and wild-type enzymes yielding a root mean square deviation of 0.220 Å over all 512 α-carbon atoms (Fig. 5*B*). In essence, the structure of the Y268A mutant in the crystal state is identical to that of the wild-type enzyme. Importantly, this demonstrates that the mutation does not alter the fold of the protein.

The quaternary structure of Y268A was next investigated using sedimentation velocity analysis in solution. Analysis using the $c(s)$ distribution (30, 31, 50) yielded a standardized sedimentation coefficient of 2.9 S, which is significantly lower than that of the wild-type enzyme at an equivalent initial protein concentration (Fig. 6*A*). Conversion of the $c(s)$ distribution to a $c(M)$ distribution shows that Y268A has an apparent molecular mass of 29.9 kDa, which correlates to a monomer (Table 3), suggesting that the propensity of the point mutant to dimerize has been significantly attenuated.

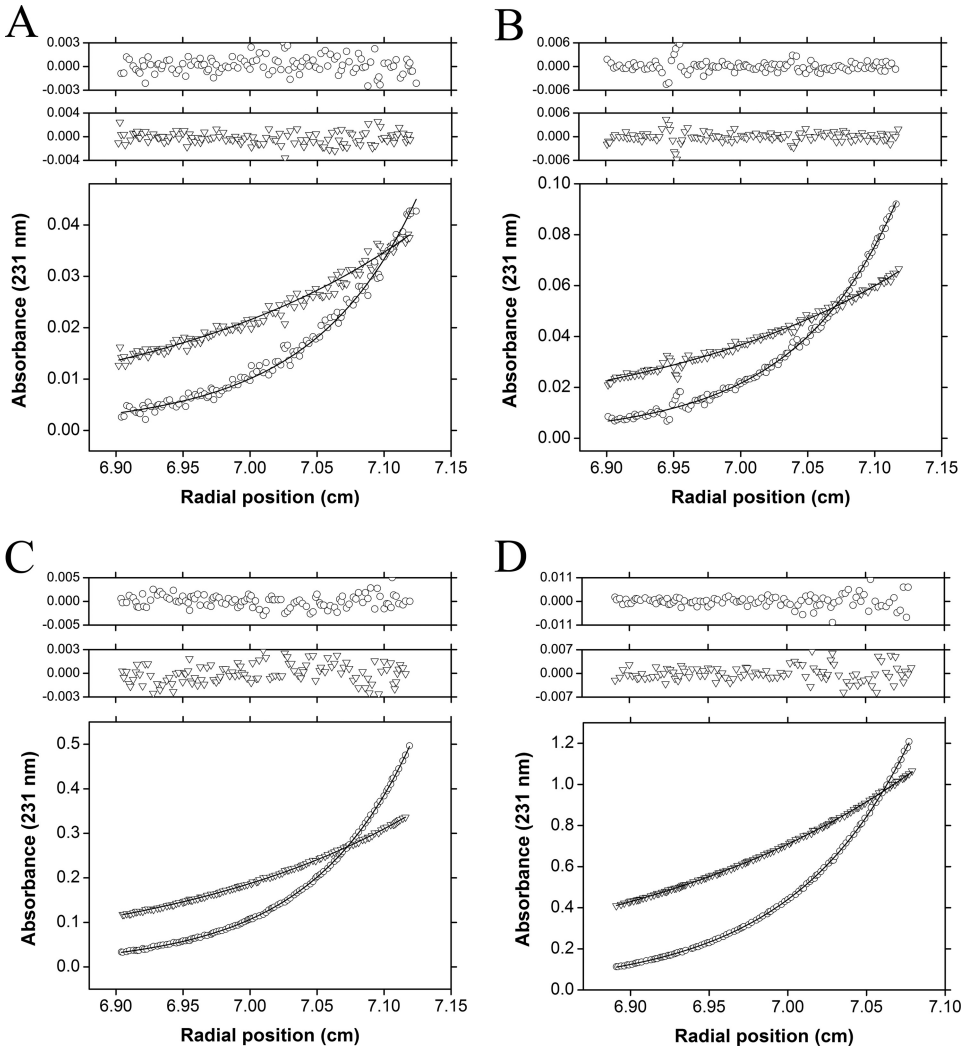

FIGURE 3. **Sedimentation equilibrium analysis of *E. coli* DAP epimerase.** Sedimentation equilibrium data collected at 10,000 (*triangles*) and 16,000 rpm (*circles*) overlaid with the global nonlinear regression best fit to a monomer-dimer self-association model (global reduced $\chi^2 = 0.104$) are shown. Residuals are displayed above each panel for 10,000 rpm data (*triangles*) and 16,000 rpm data (*circles*). The experiment was conducted at initial protein concentrations of 0.32 (*A*) 0.64 (*B*), 1.9 (*C*), and 5.8 μM (*D*), yielding a $K_D^{2\rightarrow1}$ of 22 nM.

To quantitate the loss of dimerization affinity, sedimentation equilibrium experiments were performed at various initial protein concentrations of Y268A ranging from 1.6 to 15.9 μM. The resulting data generated at two rotor speeds (10,000 and 16,000 rpm) were globally fitted to a monomer-dimer equilibrium model. The resulting global nonlinear regression best fit yielded a dimer-monomer dissociation constant ($K_D^{2\rightarrow1}$) of 54 μM (Table 3). This result indicates that the Ala substitution at position 268 has weakened the dimerization affinity by ~2,400-fold. Accordingly, the Y268A point mutant enables the structure-function relationship of a monomer to be characterized in comparison with the wild-type dimer.

Y268A Shows Attenuated Activity—The enzymatic activity of Y268A was compared with that of wild-type *E. coli* DAP epimerase by screening at a fixed concentration of 2.5 μg ml^{-1} (~80 nM). This enzyme concentration is significantly lower than the $K_D^{2\rightarrow1}$ of the Y268A point mutant but higher than the wild-type dimerization dissociation constant. Interestingly, the catalytic activity of Y268A is markedly attenuated compared with the wild-type enzyme (~1% at 80 nM enzyme concentration), which indicates that the *E. coli* DAP epimerase dimer is significantly more active than the monomeric form.

To support this inference, the relationship between catalytic activity and enzyme concentration for Y268A and wild-type enzyme was investigated. Not surprisingly, the plot of rate *versus* enzyme concentration for Y268A is nonlinear showing upward curvature, indicating that the mutant becomes more active as the enzyme concentration is increased (Fig. 6*B*). This phenomenon has been observed for other enzymes that show a dependence on quaternary structure for catalytic function (26, 27). By contrast, the plot of initial rate *versus* enzyme concentration for the wild-type enzyme is linear (Fig. 6*B*).

DISCUSSION

The DAP epimerase-fold was first identified in 1998 when the first structure of DAP epimerase from *H. influenzae* was determined (9). Since then a number of other proteins have been found to adopt this fold (13–19). Interestingly, the majority of DAP epimerase-like proteins have been reported to be

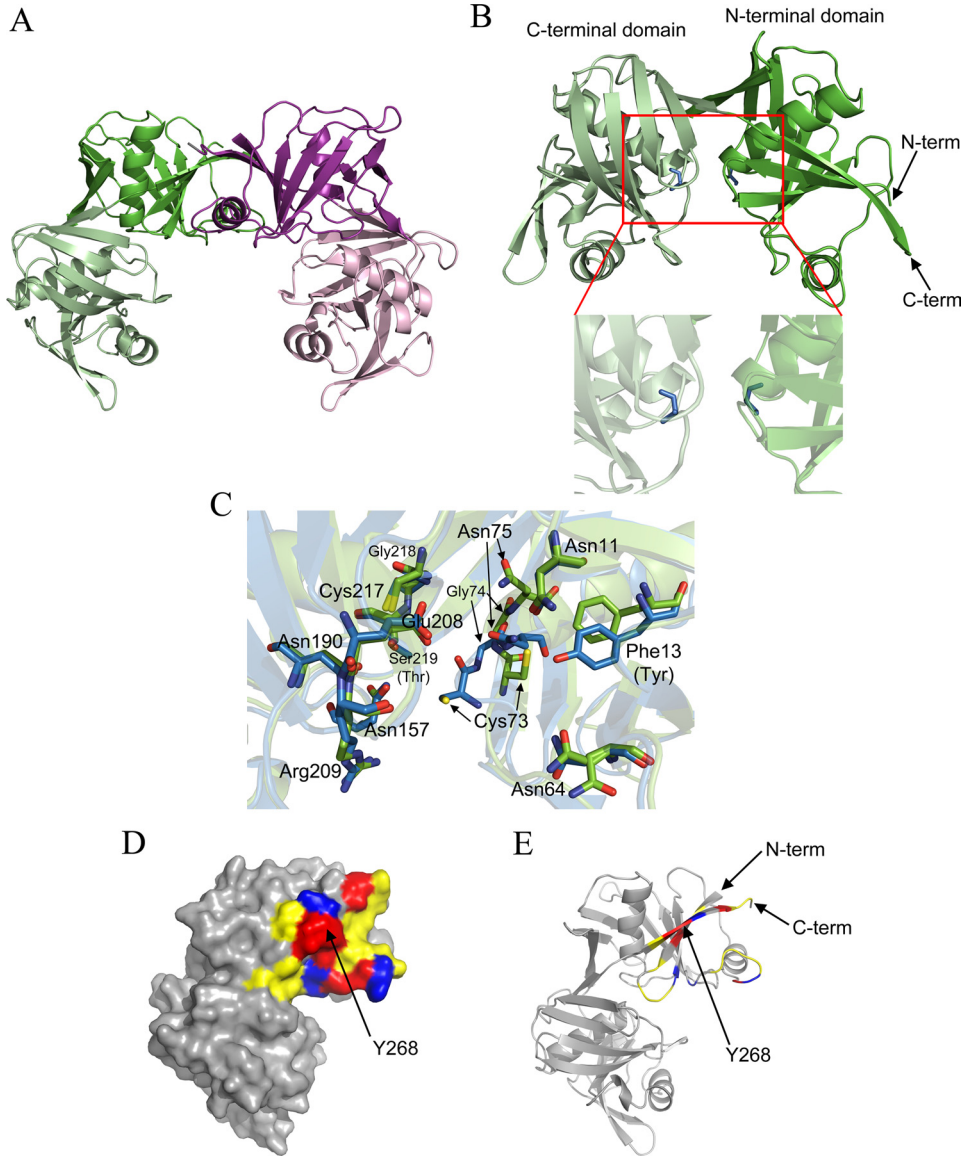

FIGURE 4. **Crystal structure of wild-type *E. coli* DAP epimerase.** *A*, dimer in the asymmetric unit. Monomers are in *green* and *purple* with the N-terminal domain in the *dark color* and the C-terminal domain in the *light color*. *B*, two symmetrical domains of *E. coli* DAP epimerase. The N-terminal domain is in *dark green*, the C-terminal domain is in *light green*, and active site Cys residues are in *blue*. *C*, overlay of the *E. coli* (Protein Data Bank code 4IJZ; *green*) and *B. anthracis* (Protein Data Bank code 2OTN; *blue*) DAP epimerase active sites. *D*, dimer interface in surface representation. *E*, dimer interface in schematic representation. Hydrogen bonds (*red*), salt bridges (*blue*), and other interface residues (*yellow*) are shown.

TABLE 4

Comparison of the dimer interface of proteins that adopt the DAP epimerase-like fold

Analysis was carried out using PISA (20).

Protein	Protein Data Bank code	Buried surface area per monomer	Buried surface area
		$Å^2$	*% of total surface area*
E. coli DAP epimerase	4IJZ	765	6.1
H. influenzae DAP epimerase (inactive)	1BWZ	688	5.6
H. influenzae DAP epimerase (open)	2Q9J	721	7.7
M. tuberculosis DAP epimerase	3FVW	1086	8.9
B. anthracis DAP epimerase	2OTN	857	5.9
Shewanella oneidensis PrpF	2PVZ	2374	14.6
Pseudomonas fluorescens PhzF	1T6K	1292	10.5
Trypanosoma cruzi proline racemase	1W62	1640	10.1
E. coli YddE	1QYA	1045	9.7

dimeric, whereas DAP epimerase enzymes have been reported to be monomeric (9, 11, 12). Accordingly, the first aim of this study was to ascertain the biologically relevant quaternary structure of DAP epimerase in solution and the crystal state.

It was determined through sedimentation analyses that both *E. coli* and *H. influenzae* DAP epimerase are in fact dimers in solution at concentrations of 100–150 μg ml^{-1} (Fig. 2). Indeed, sedimentation equilibrium analyses show that the wild-type

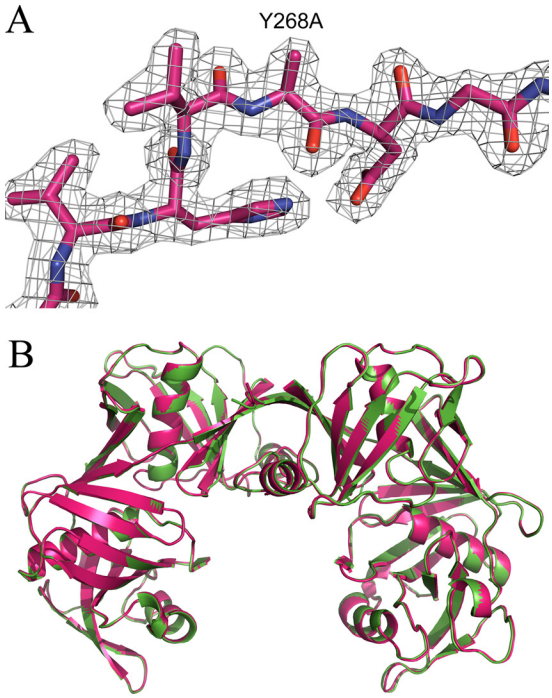

FIGURE 5. **X-ray crystal structure of Y268A.** *A*, electron density map showing atoms around the mutated residue. The $2F_o - F_c$ electron density is displayed in *gray* and contoured to 1σ. *B*, overlay of Y268A (*pink*) and wild-type *E. coli* DAP epimerase (*green*).

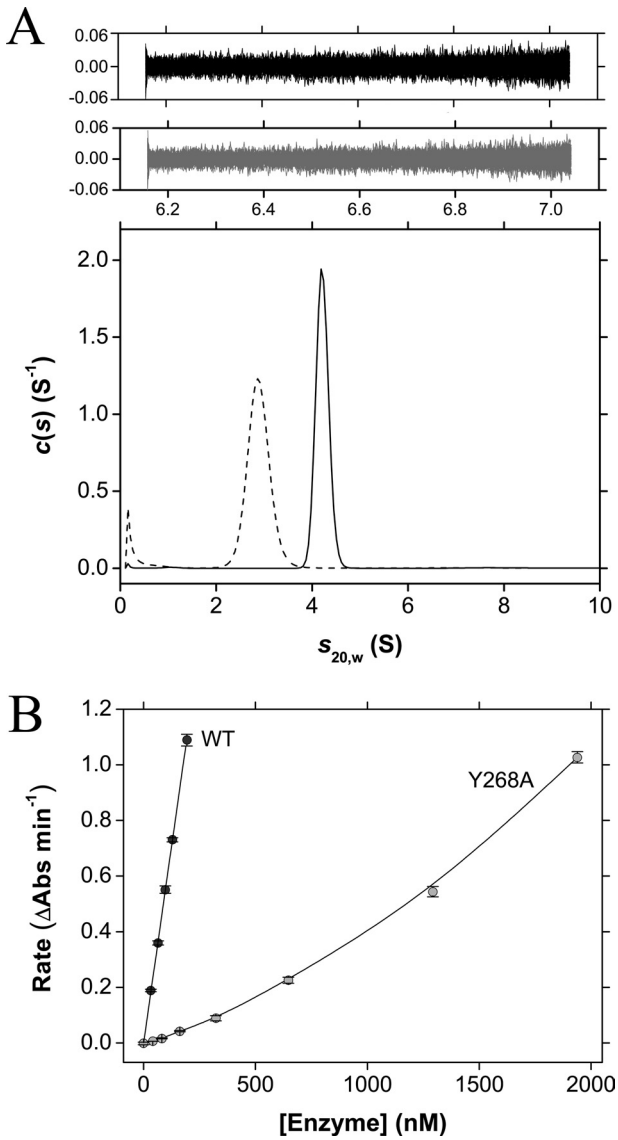

FIGURE 6. **Sedimentation velocity and catalytic activity analyses of *E. coli* DAP epimerase wild type and Y268A mutant.** *A*, continuous sedimentation coefficient (*c*(*s*)) distribution plotted as a function of sedimentation coefficient ($s_{20,w}$) for wild-type enzyme (*solid line*) and Y268A (*dashed line*). Residuals are plotted for wild-type (*black*) and Y268A (*gray*). *B*, rate *versus* enzyme concentration plots of wild-type (*dark circles*) and Y268A (*light circles*) *E. coli* DAP epimerase. The initial rate (*i.e.* change in absorbance (*Abs*)) of the DAP epimerase reaction is plotted as a function of enzyme concentration. Kinetics were performed at a LL-DAP concentration of 0.140 and 0.0246 mM for Y268A and wild-type *E. coli* DAP epimerase, respectively. *Error bars* represent the S.D. of duplicate measurements.

E. coli enzyme exists as a tight dimer with a dimer-monomer dissociation constant of 22 nM (Fig. 3 and Table 3).

In addition, the x-ray crystal structure of *E. coli* DAP epimerase determined to a resolution of 2.0 Å was crystallized in the active, open conformation, showing that the enzyme also exists as a dimer in the crystalline state (Fig. 4). The dimer adopts the same architecture observed in other proteins that adopt the DAP epimerase-like fold with dimerization facilitated by contacts in the N-terminal domain. In addition, although in previous studies *H. influenzae* DAP epimerase crystallized as a monomer in the asymmetric unit (8–10, 51), a dimer with the same architecture as that of *E. coli* DAP epimerase observed in this study (and other DAP epimerase-like fold proteins) can be generated using the appropriate symmetry operations. We believe that this dimer constitutes the catalytically active and biologically relevant form of the enzyme.

These results taken as a whole strongly suggest that DAP epimerase is in fact a dimer and that the oligomeric state of DAP epimerase has been misreported in the literature (9, 11, 12). Given that PISA analysis (20) indicates that DAP epimerase has an appreciably smaller dimer interface compared with other DAP epimerase-like proteins (Table 4), the significance of this dimerization interface and hence the oligomeric state of the protein may have been overlooked.

To probe the importance of dimerization, the crystal structure of *E. coli* DAP epimerase was used to design a monomeric mutant via site-directed mutagenesis targeting Tyr^{268}, a key residue that forms significant stabilizing interactions at the dimer interface. Results show that the mutagenesis was successful, resulting in a mutant enzyme (Y268A) with a ~2,400-fold loss in dimerization affinity compared with the wild-type enzyme (Table 3). Interestingly, enzyme kinetic analysis indicates that Y268A is significantly less active than the wild-type dimer (Fig. 6*B*). This cannot be due to loss in secondary or tertiary structure because CD spectroscopy (Table 2) and x-ray crystallography (Fig. 5) studies demonstrate that the secondary and tertiary structure of the mutant is preserved (Fig. 5). Accordingly, we propose that the loss of function found in Y268A is due to perturbation of the dimeric quaternary structure. However, because the active site in each monomer is located between the N- and C-terminal domains (Fig. 4*B*) and is distal from the dimerization interface (~22 Å between Tyr^{268} and the closest active site Cys residue), loss of func-

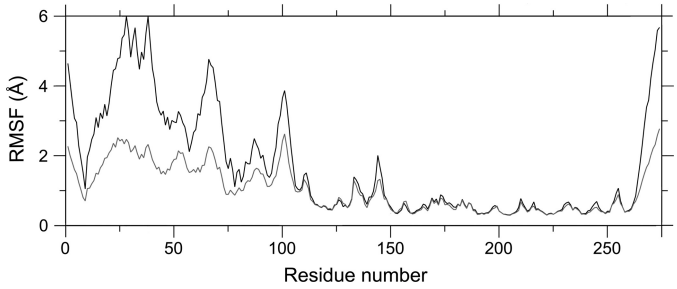

FIGURE 7. **Molecular dynamics simulations of *E. coli* DAP epimerase monomer and dimer.** The root mean squared fluctuation (*RMSF*) is plotted as a function of residue number of monomer A for the wild-type dimer (*gray line*) and monomer (*black line*). Simulations were analyzed by aligning monomer A from all frames of the trajectories and computing the root mean squared fluctuation of monomer A.

tion in the monomeric state must be due to long distance effects.

We therefore hypothesize that dimerization plays an important role in optimizing conformational dynamics critical for function. In DAP epimerase, the binding of ligand triggers a large conformational change, bringing the N- and C-terminal domains together (8, 51). This event leads to the encapsulation of ligand and the reorganization of the active site with the formation of a network of hydrogen bonds at the catalytic center and the optimal positioning of the active site Cys residues (Fig. 1) (8, 51). The correct positioning of the two active site Cys residues (Cys^{73} and Cys^{217}; *E. coli* numbering) is critical for function of the enzyme. If these two Cys residues are too far apart catalysis cannot take place; alternatively, if the two Cys residues are too close together disulfide formation will occur, rendering the enzyme inactive. Therefore, formation of the dimer is likely to aid in attenuating conformational flexibility at the interdomain junction where the active site is located to allow optimal functionality.

To test this hypothesis, molecular dynamic simulations were performed on both the monomeric and dimeric versions of DAP epimerase using the x-ray crystal structure of the *E. coli* enzyme (Protein Data Bank code 4IJZ). Preliminary results from the 25-ns simulations appear to indicate that the monomer is more flexible or "dynamic" than the dimer (Fig. 7). This is evident by the greater root mean squared fluctuations, particularly in the N-terminal domain (residues 1–119 and 263–274), when compared with the wild-type *E. coli* DAP epimerase dimer. The N-terminal domain includes a number of catalytic residues, including Cys^{73}, Gly^{74}, Asn^{75}, Asn^{11}, and Asn^{64}, and is also the dimerization domain. Thus, the buttressing of two monomers to form a dimer may prevent increased movement of the active site residues, allowing for optimal catalytic function. However, future studies using experimental approaches to measure protein dynamics are required to confirm our preliminary molecular dynamics simulation results.

Given that the findings in the study show that the monomer of DAP epimerase is significantly less active than the dimer, disruption of quaternary structure offers a new approach for the design of novel DAP epimerase inhibitors with potential antimicrobial activities. The use of small molecules or peptides to disrupt protein-protein interaction is an emerging area in drug design (54, 55). This approach has been successful in targeting homodimeric proteins, such as HIV protease and inducible nitric-oxide synthase, leading to the development of nanomolar inhibitors (53). Accordingly, the structure of *E. coli* DAP epimerase reported in this study permits structure-guided design of peptide or peptidomimetic molecules targeting the dimer interface, thus preventing dimerization of the enzyme to its active conformation.

In conclusion, this study has shown that DAP epimerase is dimeric in solution and that dimerization of the enzyme is required for optimal activity. Accordingly, our work offers insight into a new approach to aid in the development of inhibitors of DAP epimerase as novel antimicrobials.

Acknowledgments—We acknowledge the support and assistance of the friendly staff at the Bio21 Collaborative Crystallographic Centre at Commonwealth Scientific and Industrial Research Organisation Molecular and Health Technologies, Parkville, Melbourne, Australia. We thank John C. Vederas (University of Alberta) for generously providing us with the plasmid for H. influenzae DAP epimerase and members of the Perugini and Hutton laboratories for helpful discussions during the preparation of this manuscript. Part of this research was undertaken on the MX2 beamline at the Australian Synchrotron, Victoria, Australia.

REFERENCES

1. Hutton, C. A., Perugini, M. A., and Gerrard, J. A. (2007) Inhibition of lysine biosynthesis: an evolving antibiotic strategy. *Mol. Biosyst.* **3,** 458–465
2. Dogovski, C., Atkinson, S. C., Dommaraju, S. R., Hor, L., Hutton, C. A., Gerrard, J. A., Dobson, R. C. J., and Perugini, M. A. (2009) in *Biotechnology* (Doelle, H. W., and Rokem, S., eds) pp. 116–136, Eolss Publishers, Oxford, UK
3. Dogovski, C., Atkinson, S. C., Dommaraju, S. R., Downton, M., Hor, L., Moore, S., Paxman, J. J., Peverelli, M. G., Qiu, T. W., Reumann, M., Siddiqui, T., Taylor, N. L., Wagner, J., Wubben, J. M., and Perugini, M. A. (2012) in *Biochemistry* (Ekinci, D., ed) pp. 225–262, InTech Open Access Publisher, Rijeka, Croatia
4. Hutton, C. A., Southwood, T. J., and Turner, J. J. (2003) Inhibitors of lysine biosynthesis as antibacterial agents. *Mini Rev. Med. Chem.* **3,** 115–127
5. Cox, R. J., Sutherland, A., and Vederas, J. C. (2000) Bacterial diaminopimelate metabolism as a target for antibiotic design. *Bioorg. Med. Chem.* **8,** 843–871
6. Antia, M., Hoare, D. S., and Work, E. (1957) The stereoisomers of diaminopimelic acid. *Biochem. J.* **65,** 448–459
7. Wiseman, J. S., and Nichols, J. S. (1984) Purification and properties of diaminopimelic acid epimerase from *Escherichia coli. J. Biol. Chem.* **259,** 8907–8914
8. Pillai, B., Cherney, M. M., Diaper, C. M., Sutherland, A., Blanchard, J. S., Vederas, J. C., and James, M. N. (2006) Structural insights into stereochemical inversion by diaminopimelate epimerase: an antibacterial drug target. *Proc. Natl. Acad. Sci. U.S.A.* **103,** 8668–8673
9. Cirilli, M., Zheng, R., Scapin, G., and Blanchard, J. S. (1998) Structural symmetry: the three-dimensional structure of *Haemophilus influenzae* diaminopimelate epimerase. *Biochemistry* **37,** 16452–16458
10. Lloyd, A. J., Huyton, T., Turkenburg, J., and Roper, D. I. (2004) Refinement of *Haemophilus influenzae* diaminopimelic acid epimerase (DapF) at 1.75 Å resolution suggests a mechanism for stereocontrol during catalysis. *Acta Crystallogr. D Biol. Crystallogr.* **60,** 397–400
11. Usha, V., Dover, L. G., Roper, D. I., Fütterer, K., and Besra, G. S. (2009) Structure of the diaminopimelate epimerase DapF from *Mycobacterium tuberculosis*. *Acta Crystallogr. D Biol. Crystallogr.* **65,** 383–387
12. Pillai, B., Moorthie, V. A., van Belkum, M. J., Marcus, S. L., Cherney, M. M., Diaper, C. M., Vederas, J. C., and James, M. N. (2009) Crystal structure of diaminopimelate epimerase from *Arabidopsis thaliana*, an amino acid

racemase critical for L-lysine biosynthesis. *J. Mol. Biol.* **385,** 580–594
13. Buschiazzo, A., Goytia, M., Schaeffer, F., Degrave, W., Shepard, W., Grégoire, C., Chamond, N., Cosson, A., Berneman, A., Coatnoan, N., Alzari, P. M., and Minoprio, P. (2006) Crystal structure, catalytic mechanism, and mitogenic properties of *Trypanosoma cruzi* proline racemase. *Proc. Natl. Acad. Sci. U.S.A.* **103,** 1705–1710
14. Garvey, G. S., Rocco, C. J., Escalante-Semerena, J. C., and Rayment, I. (2007) The three-dimensional crystal structure of the PrpF protein of *Shewanella oneidensis* complexed with *trans*-aconitate: insights into its biological function. *Protein Sci.* **16,** 1274–1284
15. Parsons, J. F., Song, F., Parsons, L., Calabrese, K., Eisenstein, E., and Ladner, J. E. (2004) Structure and function of the phenazine biosynthesis protein PhzF from *Pseudomonas fluorescens* 2-79. *Biochemistry* **43,** 12427–12435
16. Velarde, M., Macieira, S., Hilberg, M., Bröker, G., Tu, S.-M., Golding, B. T., Pierik, A. J., Buckel, W., and Messerschmidt, A. (2009) Crystal structure and putative mechanism of 3-methylitaconate-Δ-isomerase from *Eubacterium barkeri*. *J. Mol. Biol.* **391,** 609–620
17. Blankenfeldt, W., Kuzin, A. P., Skarina, T., Korniyenko, Y., Tong, L., Bayer, P., Janning, P., Thomashow, L. S., and Mavrodi, D. V. (2004) Structure and function of the phenazine biosynthetic protein PhzF from *Pseudomonas fluorescens*. *Proc. Natl. Acad. Sci. U.S.A.* **101,** 16431–16436
18. Grassick, A., Sulzenbacher, G., Roig-Zamboni, V., Campanacci, V., Cambillau, C., and Bourne, Y. (2004) Crystal structure of *E. coli* yddE protein reveals a striking homology with diaminopimelate epimerase. *Proteins* **55,** 764–767
19. Liger, D., Quevillon-Cheruel, S., Sorel, I., Bremang, M., Blondeau, K., Aboulfath, I., Janin, J., van Tilbeurgh, H., and Leulliot, N. (2005) Crystal structure of YHI9, the yeast member of the phenazine biosynthesis PhzF enzyme superfamily. *Proteins* **60,** 778–786
20. Krissinel, E., and Henrick, K. (2007) Inference of macromolecular assemblies from crystalline state. *J. Mol. Biol.* **372,** 774–797
21. Hor, L., Dobson, R. C., Dogovski, C., Hutton, C. A., and Perugini, M. A. (2010) Crystallization and preliminary X-ray diffraction analysis of diaminopimelate epimerase from *Escherichia coli*. *Acta Crystallogr. Sect. F Struct. Biol. Cryst. Commun.* **66,** 37–40
22. Studier, F. W. (2005) Protein production by auto-induction in high density shaking cultures. *Protein Expr. Purif.* **41,** 207–234
23. Boughton, B. A., Griffin, M. D., O'Donnell, P. A., Dobson, R. C., Perugini, M. A., Gerrard, J. A., and Hutton, C. A. (2008) Irreversible inhibition of dihydrodipicolinate synthase by 4-oxo-heptenedioic acid analogues. *Bioorg. Med. Chem.* **16,** 9975–9983
24. Boughton, B. A., Hor, L., Gerrard, J. A., and Hutton, C. A. (2012) 1,3-Phenylene bis(ketoacid) derivatives as inhibitors of *Escherichia coli* dihydrodipicolinate synthase. *Bioorg. Med. Chem.* **20,** 2419–2426
25. Davis, A. J., Perugini, M. A., Smith, B. J., Stewart, J. D., Ilg, T., Hodder, A. N., and Handman, E. (2004) Properties of GDP-mannose pyrophosphorylase, a critical enzyme and drug target in *Leishmania mexicana*. *J. Biol. Chem.* **279,** 12462–12468
26. Burgess, B. R., Dobson, R. C., Bailey, M. F., Atkinson, S. C., Griffin, M. D., Jameson, G. B., Parker, M. W., Gerrard, J. A., and Perugini, M. A. (2008) Structure and evolution of a novel dimeric enzyme from a clinically-important bacterial pathogen. *J. Biol. Chem.* **283,** 27598–27603
27. Voss, J. E., Scally, S. W., Taylor, N. L., Atkinson, S. C., Griffin, M. D., Hutton, C. A., Parker, M. W., Alderton, M. R., Gerrard, J. A., Dobson, R. C., Dogovski, C., and Perugini, M. A. (2010) Substrate-mediated stabilization of a tetrameric drug target reveals Achilles heel in anthrax. *J. Biol. Chem.* **285,** 5188–5195
28. Sreerama, N., and Woody, R. W. (2000) Estimation of protein secondary structure from circular dichroism spectra: comparison of CONTIN, SELCON, and CDSSTR methods with an expanded reference set. *Anal. Biochem.* **287,** 252–260
29. Perugini, M. A., Griffin, M. D., Smith, B. J., Webb, L. E., Davis, A. J., Handman, E., and Gerrard, J. A. (2005) Insight into the self-association of key enzymes from pathogenic species. *Eur. Biophys. J.* **34,** 469–476
30. Perugini, M. A., Schuck, P., and Howlett, G. J. (2000) Self-association of human apolipoprotein E3 and E4 in the presence and absence of phospholipid. *J. Biol. Chem.* **275,** 36758–36765
31. Schuck, P. (2000) Size-distribution analysis of macromolecules by sedimentation velocity ultracentrifugation and Lamm equation modeling. *Biophys. J.* **78,** 1606–1619
32. Demeler, B., and van Holde, K. E. (2004) Sedimentation velocity analysis of highly heterogeneous systems. *Anal. Biochem.* **335,** 279–288
33. Demeler, B. (2005) in *Analytical Ultracentrifugation: Techniques and Methods* (Scott, D. J., Harding, S. E., and Rowe, A. J., eds) pp. 210–230, The Royal Society of Chemistry, Cambridge, UK
34. Demeler, B. (2005) in *Bioinformatics Basics: Applications in Biological Science and Medicine* (Buehler, L., and Rashdid, H., eds) 2nd Ed., pp. 226–255, CRC Press, Boca Raton, FL
35. Vistica, J., Dam, J., Balbo, A., Yikilmaz, E., Mariuzza, R. A., Rouault, T. A., and Schuck, P. (2004) Sedimentation equilibrium analysis of protein interactions with global implicit mass conservation constraints and systematic noise decomposition. *Anal. Biochem.* **326,** 234–256
36. Brookes, E., Demeler, B., and Rocco, M. (2010) Developments in the US-SOMO bead modeling suite: new features in the direct residue-to-bead method, improved grid routines, and influence of accessible surface area screening. *Macromol. Biosci.* **10,** 746–753
37. Brookes, E., Demeler, B., Rosano, C., and Rocco, M. (2010) The implementation of SOMO (SOlution MOdeller) in the UltraScan analytical ultracentrifugation data analysis suite: enhanced capabilities allow the reliable hydrodynamic modeling of virtually any kind of biomacromolecule. *Eur. Biophys. J.* **39,** 423–435
38. Cox, R. J., Durston, J., and Roper, D. I. (2002) Synthesis and *in vitro* enzyme activity of an oxa analogue of azi-DAP. *J. Chem. Soc. Perkin 1.* **1,** 1029–1035
39. Leslie, A. G. W. (1991) in *Crystallographic Computing 5: from Chemistry to Biology: Papers Presented at the International School in Crystallographic Computing Held at Bischenberg, France, July 29–August 5, 1990*, pp. 50–61, Oxford University Press, Inc., Oxford, UK
40. Collaborative Computational Project, Number 4 (1994) The CCP4 suite: programs for protein crystallography. *Acta Crystallogr. D Biol. Crystallogr.* **50,** 760–763
41. McCoy, A. J., Grosse-Kunstleve, R. W., Adams, P. D., Winn, M. D., Storoni, L. C., and Read, R. J. (2007) Phaser crystallographic software. *J. Appl. Crystallogr.* **40,** 658–674
42. Emsley, P., Lohkamp, B., Scott, W. G., and Cowtan, K. (2010) Features and development of Coot. *Acta Crystallogr. D Biol. Crystallogr.* **66,** 486–501
43. Winn, M. D., Murshudov, G. N., and Papiz, M. Z. (2003) Macromolecular TLS refinement in REFMAC at moderate resolutions. *Methods Enzymol.* **374,** 300–321
44. Painter, J., and Merritt, E. A. (2006) Optimal description of a protein structure in terms of multiple groups undergoing TLS motion. *Acta Crystallogr. D Biol. Crystallogr.* **62,** 439–450
45. Painter, J., and Merritt, E. A. (2006) TLSMD web server for the generation of multi-group TLS models. *J. Appl. Crystallogr.* **39,** 109–111
46. Chen, V. B., Arendall, W. B., 3rd, Headd, J. J., Keedy, D. A., Immormino, R. M., Kapral, G. J., Murray, L. W., Richardson, J. S., and Richardson, D. C. (2010) MolProbity: all-atom structure validation for macromolecular crystallography. *Acta Crystallogr. D Biol. Crystallogr.* **66,** 12–21
47. Phillips, J. C., Braun, R., Wang, W., Gumbart, J., Tajkhorshid, E., Villa, E., Chipot, C., Skeel, R. D., Kalé, L., and Schulten, K. (2005) Scalable molecular dynamics with NAMD. *J. Comput. Chem.* **26,** 1781–1802
48. MacKerell, A. D., Bashford, D., Bellott, Dunbrack, R. L., Evanseck, J. D., Field, M. J., Fischer, S., Gao, J., Guo, H., Ha, S., Joseph-McCarthy, D., Kuchnir, L., Kuczera, K., Lau, F. T. K., Mattos, C., Michnick, S., Ngo, T., Nguyen, D. T., Prodhom, B., Reiher, W. E., Roux, B., Schlenkrich, M., Smith, J. C., Stote, R., Straub, J., Watanabe, M., Wiórkiewicz-Kuczera, J., Yin, D., and Karplus, M. (1998) All-atom empirical potential for molecular modeling and dynamics studies of proteins. *J. Phys. Chem. B* **102,** 3586–3616
49. Foloppe, N., Sagemark, J., Nordstrand, K., Berndt, K. D., and Nilsson, L. (2001) Structure, dynamics and electrostatics of the active site of glutaredoxin 3 from *Escherichia coli*: comparison with functionally related proteins. *J. Mol. Biol.* **310,** 449–470
50. Schuck, P., Perugini, M. A., Gonzales, N. R., Howlett, G. J., and Schubert, D. (2002) Size-distribution analysis of proteins by analytical ultracentrif-

ugation: strategies and application to model systems. *Biophys. J.* **82,** 1096–1111
51. Pillai, B., Cherney, M., Diaper, C. M., Sutherland, A., Blanchard, J. S., Vederas, J. C., and James, M. N. (2007) Dynamics of catalysis revealed from the crystal structures of mutants of diaminopimelate epimerase. *Biochem. Biophys. Res. Commun.* **363,** 547–553
52. Koo, C. W., and Blanchard, J. S. (1999) Chemical mechanism of *Haemophilus influenzae* diaminopimelate epimerase. *Biochemistry* **38,** 4416–4422
53. Cardinale, D., Salo-Ahen, O. M. , Ferrari, S., Ponterini, G., Cruciani, G., Carosati, E., Tochowicz, A. M., Mangani, S., Wade, R. C., and Costi, M. P. (2010) Homodimeric enzymes as drug targets. *Curr. Med. Chem.* **17,** 826–846
54. Wells, J. A., and McClendon, C. L. (2007) Reaching for high-hanging fruit in drug discovery at protein-protein interfaces. *Nature* **450,** 1001–1009
55. Gerrard, J. A., Hutton, C. A., and Perugini, M. A. (2007) Inhibiting protein-protein interactions as an emerging paradigm for drug discovery. *Mini Rev. Med. Chem.* **7,** 151–157